Journal of Applied Polymer Science

UV-Cured Cellulose Nanofiber Composites with Moisture Durable Oxygen Barrier Properties

Sylvain Galland,[1,2,3] Yves Leterrier,[3] Tommaso Nardi,[3] Christopher J. G. Plummer,[3] Jan Anders E. Månson,[2] Lars A. Berglund[1,2]

[1]Department of Fiber and Polymer Technology, School of Chemical Science and Engineering, Royal Institute of Technology (KTH), 10044 Stockholm, Sweden

[2]Wallenberg Wood Science Center (WWSC), Royal Institute of Technology (KTH), 10044 Stockholm, Sweden

[3]Laboratoire de Technologie des Composites et Polymères (LTC), Ecole Polytechnique Fédérale de Lausanne (EPFL), CH-1015 Lausanne, Switzerland

Correspondence to: Y. Leterrier (E-mail: yves.leterrier@epfl.ch)

ABSTRACT: Nanocomposites based on 10 to 60 vol % cellulose nanofibers (NFC) in a photopolymerizable hyperbranched acrylate matrix were prepared. Unmodified NFC and NFC chemically modified with a silane coupling agent and with ceric ammonium nitrate for direct polymer grafting from the cellulose surface were used. A homogeneous dispersion of NFC in the matrix was obtained in each case, leading to a marked improvement in oxygen barrier (up to nine times) and thermomechanical properties (storage modulus increased up to seven times). The mechanisms involved in the permeability reduction were investigated, revealing non-monotonic trends in the evolution of the solubility and diffusion coefficients with NFC content. Most significantly, the inherent moisture sensitivity of the oxygen permeability of the NFC was found to be drastically reduced when it was dispersed in the polymer matrix, particularly after chemical modification, underlining the promise of the present approach for the production of robust, high barrier organic films. © 2014 Wiley Periodicals, Inc. J. Appl. Polym. Sci. **2014**, *131*, 40604.

KEYWORDS: cellulose and other wood products; mechanical properties; nanoparticles; nanowires and nanocrystals; photopolymerization; surfaces and interfaces

Received 21 January 2014; accepted 14 February 2014
DOI: 10.1002/app.40604

INTRODUCTION

Materials that provide an efficient barrier to oxygen and other gases are a key component in applications such as food packaging, electronic devices and fuel cells.[1–3] In many cases, the barrier film is also required to show adequate optical transparency, resist mechanical loads/deformations and be sufficiently durable with respect to for example, fatigue or weathering. Various approaches to meeting these requirements have been investigated, based mainly on combining mechanically tough polymers with ultra-low-permeability inorganic compounds. This is typically achieved by either bulk mixing of the two components to form a thin nanocomposite film,[2] or preparation of a multilayer coating comprising an intrinsically impermeable phase with a high aspect ratio such as graphene oxide.[3] However, bulk mixing may result in nanoparticle aggregation and a consequent loss in barrier properties and transparency, while in multilayer structures, the brittle inorganic layers may crack at low applied strains, again resulting in a loss in barrier properties.[4] Introduction of additional layers may improve the performance of multilayer films, but entails a considerable increase in production costs.

It follows that the development of novel economically viable materials with the potential to overcome these problems is of major importance. At the same time, however, respect for society's expectations with regard to the environment places additional constraints on the development of any novel materials solution. Nanofibrillar cellulose (NFC), extracted from low-cost widely available natural resources such as wood, has already shown great potential in polymer nanocomposites (allowing one to combine e.g. mechanical reinforcement and optical transparency).[5–7] More recently,[8–10] it has also been shown that dense NFC networks ("nanopaper") provide excellent gas barrier properties, owing to their high degree of crystallinity and density of hydrogen bonds, although such systems are currently limited by their moisture sensitivity, as reflected by severe degradation in their barrier properties at high relative humidity.[8,11–13]

In spite of the promise of NFC as a barrier material, to date little effort has been made to exploit its barrier properties in

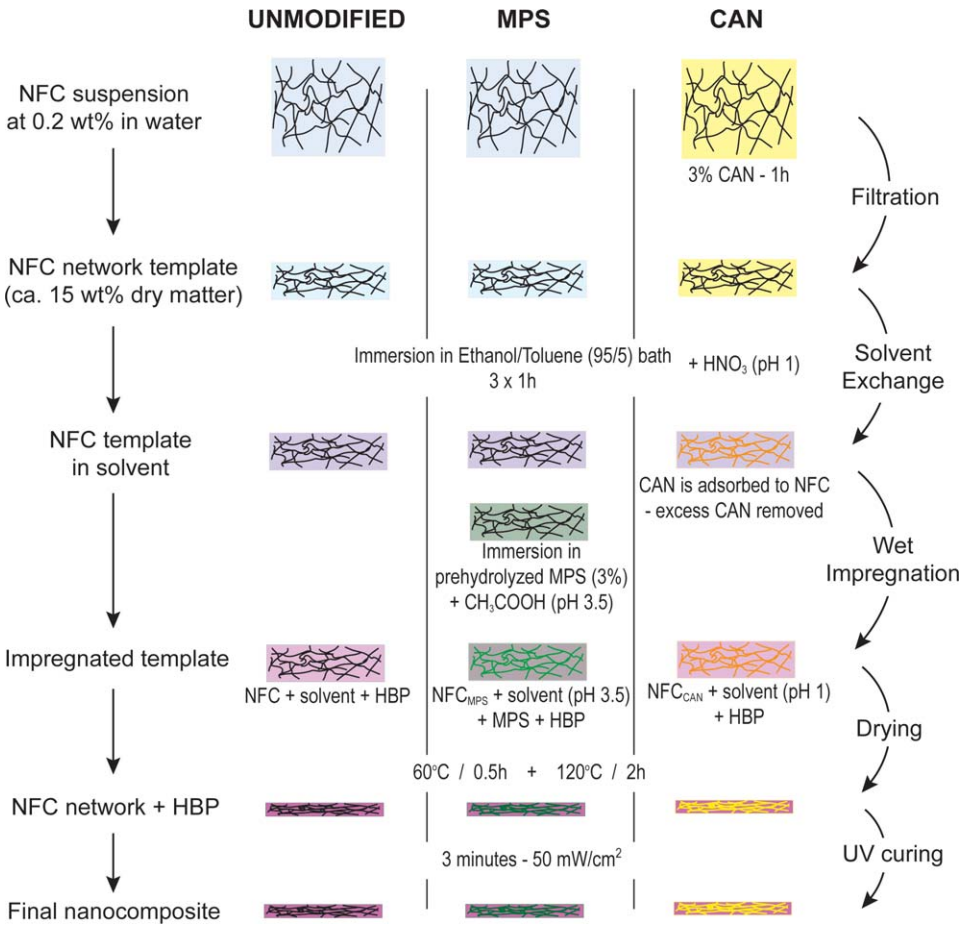

Figure 1. Summary of the impregnation routes for NFC-HBP nanocomposites with different cellulose treatments. [Color figure can be viewed in the online issue, which is available at wileyonlinelibrary.com.]

combination with a polymer matrix. Aulin et al.[9] recently reported layer-by-layer deposition of NFC and a polyelectrolyte to form barrier coatings on poly(lactic acid) films. This approach led to low permeability at 50% RH, but the barrier properties were substantially lost at higher humidity owing to the hygroscopicity of the charged polyelectrolyte and NFC layers. Moreover, the layer-by-layer approach, which requires multiple dip-washing steps, is time-consuming and difficult to adapt to large-scale continuous production. Plackett et al.[14] mixed NFC with water-soluble amylopectin and prepared cast films. A strong decrease in the oxygen permeability was again observed in the dry films. However the moisture sensitivity was not investigated in this case and extensive aggregation of the NFC took place during casting. Such aggregates are expected to result in excessive moisture uptake and loss of barrier properties at high humidity levels, and indeed are generally characteristic of processing routes involving direct mixing of the components in aqueous suspension.[15] Moreover, the hydrophilic NFC is difficult to disperse in organic solvents, so that aggregation becomes even more problematic when preparing nanocomposites from water insoluble polymers. Henriksson et al. demonstrated the potential of a wet impregnation route for preparing NFC nanocomposites with a hyperbranched polymer matrix.[16] Ansari et al.[17] have subsequently used a similar template approach with solvent exchange and impregnation to obtain a highly homogeneous NFC dispersion in a thermoset epoxy matrix. The resulting films contain well separated fibrils, and absorb relatively small amounts of moisture, so that mechanical properties are maintained under humid conditions.

In the present work, we have investigated the oxygen barrier properties of a series of NFC nanocomposite films prepared by adapting the wet template impregnation route for use with a hyperbranched photopolymerizable (HBP) matrix. Acrylated HBP resins have the advantages of low viscosity and very high cure rates (a few seconds under UV irradiation are sufficient to obtain a high degree of cure), which make them suitable for cost-effective processing of films and coatings. Moreover, considerable efforts are presently paid to reduce the production costs of NFC.[18] Altogether, these characteristics are highly relevant to future potential practical applications of NFC nanocomposites, allowing one to envisage adaptation of the laboratory-scale wet impregnation route to a continuous roll-to-roll process (similar to paper forming), taking advantage of the rapidity of the UV cure. There is nevertheless little existing literature on UV-cured NFC nanocomposites.[19] We have also explored the possibility of chemically modifying the NFC surface in the preformed template nanofibril network by either adsorption of a

methacrylated silane coupling agent, or direct grafting of HBP oligomers, with the aim of reducing sensitivity of the oxygen permeability of the final nanocomposites to moisture.

EXPERIMENTAL

Materials

Cellulose nanofibrils were extracted from bleached industrial softwood sulfite pulp (13.8 wt % hemicellulose, 0.7 wt % lignin) according to the procedure of Henriksson et al.[20] Briefly, the pulp fibers were treated with an enzyme solution (0.25 wt % Novozyme 476 for 2 h at 50°C) to facilitate mechanical fibrillation of the cell wall. The nanofibrillated cellulose (NFC) was collected after eight passes through a microfluidizer (M-110EH, Microfluidics Ind.) as an aqueous gel-like suspension (2 wt % dry content). The hyperbranched polymer (HBP) resin used in this work was a hyperbranched polyester acrylate oligomer provided by Sartomer (CN2302) with an acrylate equivalent weight of 122 g mol^{-1}; 2,4,6-trimethylbenzoyl-diphenyl-phosphineoxide (TPO) was used as photoinitiator and 6 wt % TPO was added to the CN2302 oligomer. This formulation was used as the resin throughout this work, and will hereafter be referred to as "HBP." A mixture of ethanol-toluene (95 : 5 by weight) was used to dissolve the HBP and will hereafter be referred to as the "solvent." The following chemicals were used for the cellulose nanofibril modification: 3-[(methacryloxy)propyl]trimethoxysilane (MPS), ceric ammonium nitrate (CAN), acetic acid, and nitric acid, all provided by Sigma Aldrich (ACS reagent grade).

Three different types of nanocomposites were prepared as shown schematically in Figure 1 and as described in what follows.

Processing of Neat NFC Nanocomposites. A given amount of the NFC suspension was diluted to 0.2 wt % in deionized water and subjected to high-shear stirring (Ultraturrax) for 10 min. The suspension was then degassed in a vacuum chamber for 20 min. A wet NFC network template was formed (hydrogel with ca. 15 wt % dry matter) by vacuum filtration using a membrane with 0.65 μm pores (Millipore). This template was dipped in a solvent bath (mixture of ethanol-toluene, 95 : 5 by weight) for 1 h at room temperature and the operation repeated three times with fresh solvent to ensure complete solvent exchange. The template was then dipped in a bath containing the HBP dissolved in the solvent (at a given concentration) and left for 2 h to allow diffusion of the resin (template thickness 100–500 μm). After impregnation, the solvent was evaporated in an oven at 60°C for 30 min followed by 2 h at 120°C. Finally, the resulting nanocomposite film (thickness 60–120 μm) was polymerized under UV radiation for 3 min at an intensity of 50 mW/cm^2 using a 200 W mercury bulb UV lamp (OmniCure 2000, Exfo, Canada). The light intensity was measured using a calibrated radiometer (Silver Line, CON-TROL-CURE, Germany), between 230 and 410 nm.

The initial amount of NFC and the HBP concentration in the impregnation bath were chosen based on preliminary trials so as to give nanocomposites containing 10, 40, and 60 vol % NFC. The composition was verified based on the known NFC mass introduced into the material and the measured final mass of the nanocomposite. The conversion from the measured wt % to vol % was obtained using densities of 1.45 and 1.21 g cm^{-3} for the NFC[21] and HBP, respectively.

Processing of MPS-Modified NFC Nanocomposites. A silane coupling agent with methacrylate functionality (MPS) was used to improve the compatibility between the hydroxyl rich NFC surface and the acrylate polymeric matrix. Organosilane treatment has been used extensively for improving interface properties in cellulose fiber/polymer composites.[22,23] More recently, this approach was extended to modify cellulose nanofibers in suspension.[24] Here the silane treatment was adapted to the template impregnation procedure, i.e. the modification was applied to the preformed nanofiber network rather than to a suspension of individual fibers. The processing route was the same as described above for neat NFC nanocomposites, but with the following modifications: after solvent exchange, the NFC template was dipped in a pre-hydrolyzed MPS solution. The solution was prepared by adjusting the pH of the solvent to 3.5 with acetic acid, and adding 3 wt % of MPS. After stirring for 1 h at room temperature, the template was immersed in the solution and left for 1 h to allow diffusion of the MPS to the NFC surface and adsorption. The required amount of HBP was then added and allowed to diffuse for another 2 h. Drying and cure were carried out as described above. Previous work[22–25] has shown it to be necessary to provide sufficient heat to condense the silanol groups with the cellulose hydroxyl groups and form a covalent linkage between the coupling agent and the cellulose. In the present case, as will be discussed in the results section, the drying step of 2 h at 120°C was sufficient for this purpose.

Processing of CAN-Modified NFC Nanocomposites. Several authors have demonstrated the possibility of using ceric ammonium nitrate (CAN) to initiate polymerization/grafting of acrylate monomers from cellulosic surfaces.[26] The mechanism involves formation of an organometallic chelate, enabling the opening of the cellulose glucose ring, particularly in acidic media.[27,28] UV radiation has also been shown to accelerate significantly the rate of the reaction initiated by CAN.[29] Therefore, in the present work, CAN was first adsorbed to the cellulose nanofibril surfaces by adding 3 wt % of CAN to the dilute NFC aqueous suspension (0.2 wt % dry content in water) and stirring at room temperature for 1 h. The same procedure was subsequently followed as for the neat NFC nanocomposites, except that the solvent was adjusted throughout to pH 1 using nitric acid. The solvent exchange procedure in this case acts as a washing step, removing any free CAN molecules not adsorbed to the NFC. The acidic conditions also favored grafting reaction of the cellulose with the HBP even under ambient conditions and before UV irradiation, as will be discussed further in the results section.

Fourier-Transform Infra Red (FT-IR) Spectroscopy

The effectiveness of the MPS and CAN treatments was evaluated using FT-IR. For the silane coupling agent (MPS), a specimen was prepared as described previously, but without introduction of HBP, i.e. the specimen was dried directly after impregnation with MPS solution. The effect of drying temperature was

investigated by preparing a specimen dried at 120°C and a specimen dried at room temperature. Both specimens were then thoroughly washed with the solvent (several days in a solvent bath with regular solvent exchange) to remove unbound MPS. The presence of MPS bound to the NFC surface was revealed by the carbonyl peak (C=O stretch at ca. 1720 cm^{-1}), which is absent for neat NFC. For the CAN initiated grafting, specimens were prepared according to the procedure described previously. However the HBP was used without any photoinitiator, so that polymerization could only occur in these specimens if initiated by the adsorbed CAN. A specimen was also shielded from the UV radiation for comparison. After processing, all the specimens were washed thoroughly with the solvent and analyzed by FT-IR spectroscopy. The carbonyl adsorption band was again used to detect the presence of HBP bound to the cellulose fibrils.

Rheology of Impregnated Templates

Specimens containing 10 vol % of NFC (modified and unmodified) were analyzed before UV cure in a rheometer (AR 2000, TA Instruments) in the parallel disc configuration (25 mm diameter). The 250 μm thick specimens were subjected to a dynamic shear strain with an amplitude of 1% and the frequency was varied from 10^{-2} to 10^{2} Hz. All measurements were made at room temperature (23°C).

Photocalorimetry

In order to establish the effect of NFC with different modifications on the HBP photo-polymerization kinetics, a photocalorimetric study was carried out. Impregnated specimens with different compositions and different treatments were prepared. Photopolymerization of the specimens was initiated immediately after drying in a photo-differential scanning calorimeter (photo-DSC, Q100 TA Instruments). The UV source was adjusted to illuminate the DSC chamber with an intensity of 50 mW cm^{-2} and the heat flux was recorded over 2 min at a constant temperature of 30°C. The conversion, α, was calculated based on the measured and theoretical exotherms for the acrylate reaction [eq. (1)],[29,30]

$$\frac{d\alpha}{dt}(t)=\frac{H_{HBP}(t)}{H_{th}}=\frac{H_{meas}(t)}{\Delta H_{acr}}\cdot\frac{AEW}{w_{HBP}} \quad (1)$$

where H_{meas} is the measured heat flux per gram, ΔH_{acr} is the energy of the acrylate double bond[31] equal to 86.31 kJ mol^{-1} for the HBP and 54.89 kJ mol^{-1} for the MPS, w_{HBP} is the weight fraction of HBP (or MPS) in the nanocomposite, and AEW is the acrylate equivalent weight (122 g mol^{-1} for HBP and 248.35 g mol^{-1} for MPS). The equation was adapted to take into account the presence of MPS in the modified template, supposing MPS and HBP are reacting simultaneously and with the same speed.

Dynamic Mechanical Thermal Analysis (DMTA)

Rectangular strips 3 to 4 mm wide and 70 to 100 μm thick were cut from the films and tested in the DMA Q800 analyzer (TA Instruments) in tensile mode (ca. 10 mm span length). Measurements were performed at a frequency of 1 Hz with a temperature ramp from 0 to 180°C at a constant heating rate of 3 K min^{-1}.

Scanning Electron Microscopy (SEM)

Cross-sections were prepared for SEM analysis by tensile fracture at room temperature (23°C). The freshly fractured surfaces were sputtered with about 15 nm thin layer of carbon (Cressington sputter coater 108) and then observed with a field-emission gun SEM (FEI XL-30, Philips).

Thermogravimetric Analysis (TGA)

The thermal degradation of the different nanocomposite materials was analyzed under oxygen flow (50 mL min^{-1}). The temperature was first maintained for 5 min at 120°C to remove any adsorbed moisture. Then the mass loss was recorded during temperature scans up to 500°C at a constant rate of 10 K min^{-1}.

Oxygen Permeability Measurements

Identical nanocomposite specimens were mounted in the two parallel chambers of an oxygen permeation analyzer (Systech 8001, accuracy of 8×10^{-3} cm^3 m^{-2} day^{-1} bar^{-1}), using a steel mask with a circular opening of 5 cm^2. The chambers were purged with nitrogen until baseline stabilization and the permeation test was then initiated by exposing one side of the film to a flow of pure oxygen gas.[1] The steady-state oxygen transmission rate (OTR [cm^3 m^{-2} day^{-1}·0.1 MPa^{-1}]) was recorded at five different temperatures (10, 20, 30, 40, and 50°C) under totally dry conditions and at 50% RH. The OTR was also recorded at different relative humidities (0, 30, 50, 65, and 80% RH) at a constant temperature of 23°C. The oxygen permeability (P) was then expressed in units of cm^3 μm m^{-2} day^{-1} kPa^{-1}. The time-lag method was used to determine apparent diffusion and solubility coefficients from the transient and steady state contributions to permeation.[32] The recorded oxygen flux was integrated to give the total volume of oxygen transmitted through unit area of the membrane as a function of time. The time-lag t_0 was then determined graphically, and the diffusion coefficient D calculated from eq. (2),[32]

$$D=\frac{L^2}{6\cdot t_0} \quad (2)$$

where L is the film thickness. The solubility coefficient (the reciprocal Henry's law coefficient) may then be derived from eq. (3) for the permeability,

$$P=D\cdot S \quad (3)$$

Dynamic Vapor Sorption (DVS) Measurements

The moisture uptake of each nanocomposite material was recorded at 33°C for different relative humidities (0, 30, 50, 65, and 80% RH) starting from the completely dry state. A DVS apparatus from Surface Measurement Systems was used. The samples were maintained at each level of humidity until equilibration of the mass (generally after 1 to 2 days).

RESULTS AND DISCUSSION

NFC Modification with MPS as a Coupling Agent or by CAN-Initiated Grafting

A strong absorption peak corresponding to the C=O stretching was observed in specimens modified with both MPS and CAN even after thorough washing with the solvent [Figure 2(a)]. In the MPS-modified NFC, the presence of the C=O band

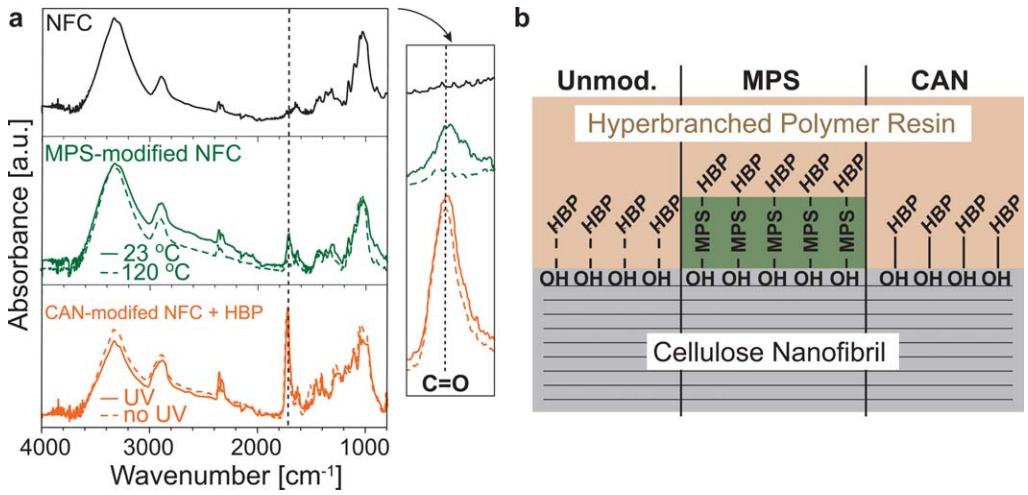

Figure 2. (a) FT-IR spectra of unmodified NFC, MPS-modified NFC for the drying temperatures indicated, and CAN-modified NFC with and without UV exposure (the specimens were washed thoroughly with solvent to remove any unbound molecules); (b) schematic of the NFC-HBP interface after different chemical treatments (dashed lines for H-bonds; continuous lines for covalent bonds). [Color figure can be viewed in the online issue, which is available at wileyonlinelibrary.com.]

assigned to the methacrylate group of MPS confirmed the formation of permanent linkages between the silane coupling agent and the NFC surface, provided a sufficiently high temperature was used during drying (120°C). Indeed, in the specimen dried at room temperature, the MPS was completely removed by washing (in this case the MPS was only physically adsorbed to the NFC surfaces through hydrogen bonding). For the CAN-modified sample, the sharp C=O band indicates that multifunctional acrylate oligomers were successfully attached to the NFC surface via permanent bonds. Exposure to UV radiation was therefore not required to form permanent linkages between the HBP and the CAN-modified NFC, with a strong C=O band being observed in both cases. It follows that the presence of CAN at the NFC surface and under acidic conditions provided favorable conditions for the grafting of acrylate oligomers to the cellulose.

The three different types of nanocomposite prepared in this work could hence be differentiated based on the nature of the matrix/NFC interface [Figure 2(b)]. In the unmodified NFC nanocomposites, the hydroxyl functionalized cellulose surface was potentially able to form hydrogen bonds with the acrylic polymer matrix. In the nanocomposites with MPS-modified NFC, the silane was successfully bound to the cellulose fibrils, and could hence potentially react covalently with the methacrylate groups of the HBP. Finally, the nanocomposites with CAN-modified NFC were expected to contain direct covalent links between the NFC and the HBP matrix.

Rheology of the Nanocomposites Before UV-Cure

Even at the lowest NFC content (10 vol %) the impregnated templates already formed solid gels before photo-polymerization owing to the percolating nanofibril network. η^* was roughly proportional to the reciprocal of the angular frequency, ω, in these gels (Figure 3), as reported previously for aqueous NFC,[34] i.e. an essentially elastic response, which was assumed to be dominated by that of the NFC network given the relatively low viscosity and Newtonian behavior of the uncured HBP. However, while the templates containing neat and MPS-modified NFC showed similar η^* at a given ω, as one might expect, given that surface treatment should not significantly influence the fibril stiffness, treatment with CAN led to somewhat higher η^*. CAN has already been argued to initiate grafting reactions under ambient conditions before UV irradiation [cf. Figure 2(a)], so that the higher η^* observed for CAN-modified NFC were attributed to polymerization of the HBP.

Photocalorimetric Study of Nanocomposite Polymerization

The photocalorimetric measurements all revealed rapid polymerization under UV irradiation with most of the conversion being achieved after less than 10 s. The reaction kinetics are shown in Figure 4, where the conversion rate is plotted against conversion, α. For all the materials, the form of the curves was

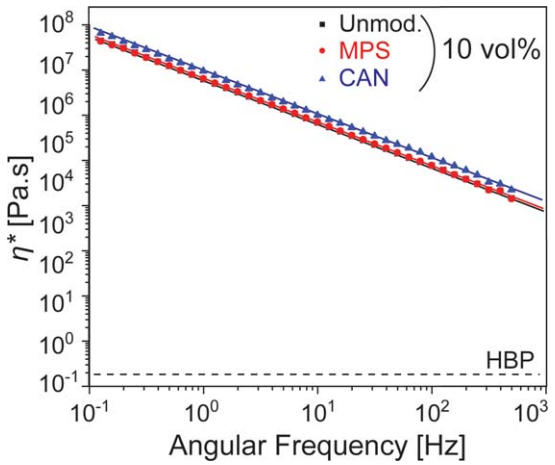

Figure 3. Complex viscosity as a function of angular frequency for non-irradiated nanocomposite specimens containing 10 vol % of NFC subjected to different chemical treatments, and for the reference HBP.[33] [Color figure can be viewed in the online issue, which is available at wileyonlinelibrary.com.]

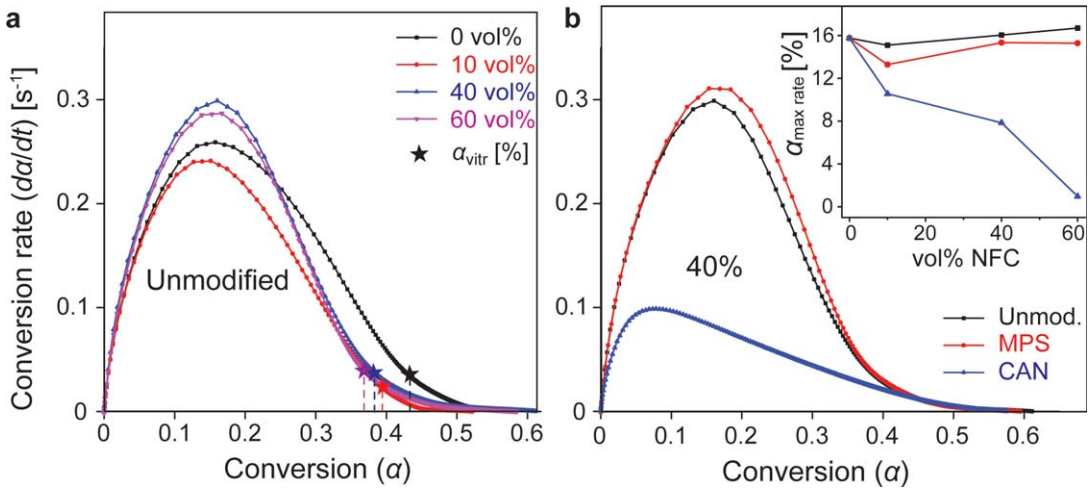

Figure 4. Conversion rate as a function of conversion for the photopolymerization of nanocomposites with (a) different amounts of neat NFC, and (b) with various NFC treatments at 40 vol % loading. The inset shows the dependence of the degree of conversion corresponding to the maximum rate of conversion on NFC content for the different treatments. [Color figure can be viewed in the online issue, which is available at wileyonlinelibrary.com.]

characteristic of an autocatalyzed reaction, which may be expressed by eq. (4)[35]

$$\frac{d\alpha}{dt} = K \cdot \left(\frac{\alpha}{\alpha_{vitr}}\right)^m \cdot \left(1 - \frac{\alpha}{\alpha_{vitr}}\right)^n \quad (4)$$

where m and n are the autocatalytic exponent and the reaction order, respectively, K is the rate constant of the reaction, and α_{vitr} the conversion rate at vitrification.[36] Values for the different parameters obtained by curve fitting are listed in Table I.

The inclusion of neat NFC in the HBP did not significantly affect the cure kinetics [Figure 4(a)], with the exception of a reduction in α_{vitr} with respect to that of the neat resin. The early stage of the reaction (at low conversions) was governed by the free radical photoinitiation mechanism,[29] which was apparently not influenced by the presence of even large amounts of NFC (up to 60 vol %). This indicates sufficient transparency of NFC to the UV light to let the photons penetrate the thickness of the nanocomposite films and interact with the photoinitiator to create free radicals.

Similar behavior was observed in the MPS-modified specimens [Figure 4(b)], suggesting no significant influence from the presence of MPS at the cellulose fibril surfaces on the polymerization kinetics. In contrast, the specimens with CAN-modified NFC showed a significant reduction in conversion rates and a shift in the conversion rate peak towards lower α [Figure 4(b) and inset]. This is presumably because a certain amount of polymerization had already taken place before the photocalorimetric experiments, as implied by the FT-IR and rheological studies, with CAN acting as a free radical initiator. Because CAN was adsorbed at the NFC surface, the extent of polymerization before UV irradiation was greater for the nanocomposites with higher contents of modified NFC.

Note that there was no visible degradation of the cellulosic materials under these UV exposure conditions (no discoloration). While general mechanisms for the photodegradation of cellulose molecules through free radical formation are well documented,[37,38] no relevant quantitative data could be found in the literature for the specific case of cellulose nanofibrils and the study of NFC photo-degradation is beyond the scope of this work.

Nanocomposite Morphology

The fracture surfaces of the various nanocomposites are shown in Figure 5. The white dots visible in the micrographs correspond to the ends of individual NFC fibrils extending from the fracture plane. The nanocomposites containing 10 vol % of NFC all showed a homogeneous through-thickness dispersion of the nanofibrils [Figure 5(a,c,e)]. The roughness of the surface

Table I. Coefficients Obtained by Fitting eq. (4) to the Photocalorimetric Results for the Different Materials Studied

NFC fraction (vol %)	$\alpha_{max\ rate}$	α_{max}	α_{vitr}	K (s^{-1})	m	n	$m+n$
0%	0.16	0.58	0.43	0.76	0.65	1.02	1.67
10%	0.15	0.52	0.39	0.77	0.69	1.13	1.82
40%	0.16	0.61	0.38	0.99	0.74	1.12	1.86
60%	0.17	0.59	0.37	0.94	0.75	1.06	1.81
40% MPS	0.15	0.6	0.38	1.04	0.77	1.06	1.83
40% CAN	0.08	0.58	0.50	0.22	0.38	1.47	1.85

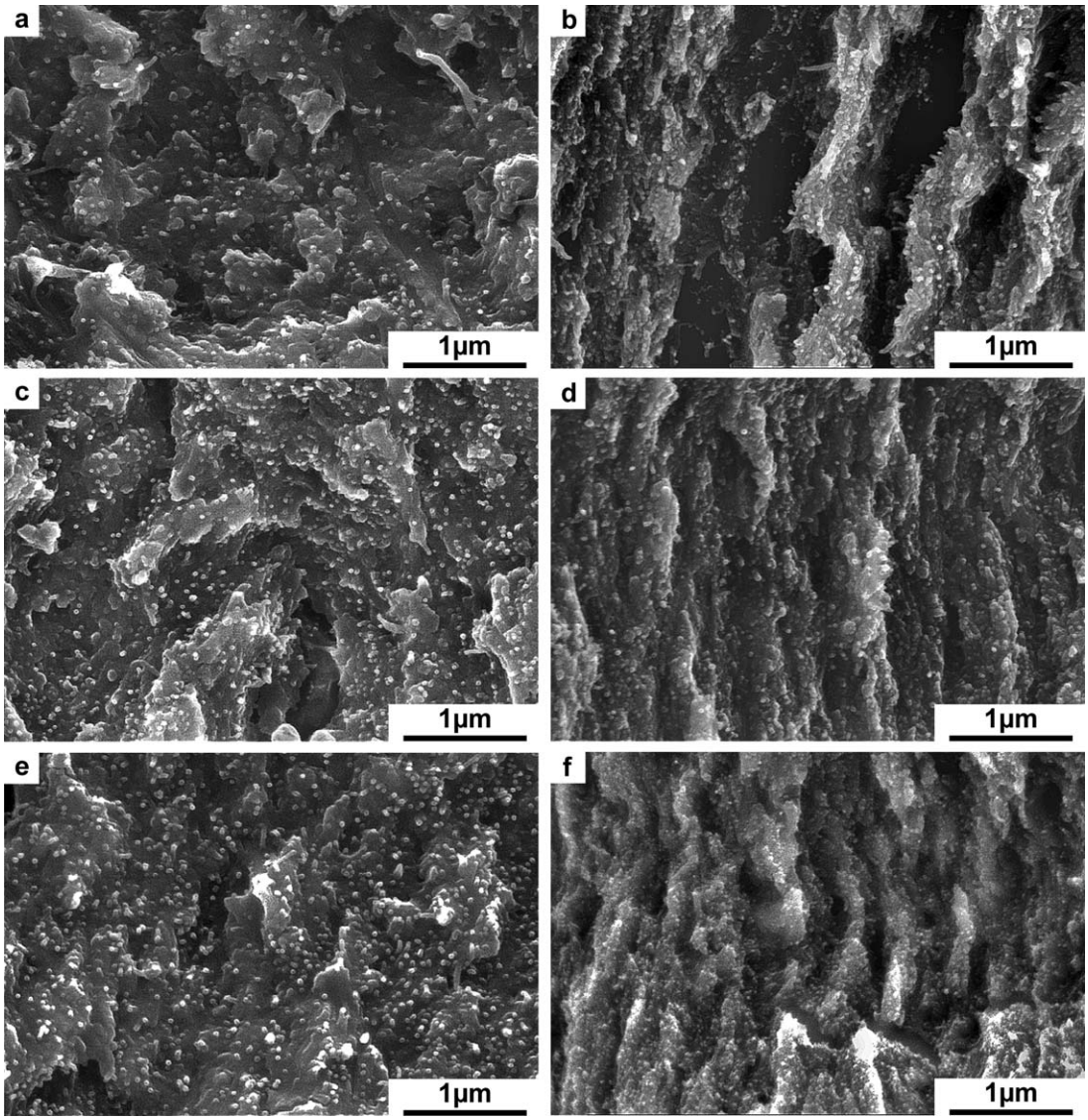

Figure 5. Scanning electron micrographs of fracture surfaces from nanocomposites containing 10 vol % (a, c, e) and 60 vol % (b, d, f) of unmodified (a, b), MPS-modified (c, d), and CAN-modified (e, f) NFC.

suggested a ductile mode of fracture, and the apparently short fibril pull-out length indicated good compatibility and stress-transfer between the polymer matrix and cellulose fibrils. No significant differences were seen after NFC treatment in the specimens containing 10 vol % NFC.

At higher NFC contents [Figure 5(b,d,f)] the layered structure characteristic of the present NFC processing route became more obvious from the fracture surfaces. Aggregated sheets are commonly observed in neat NFC-based nanopaper, and result in strong two-dimensional anisotropy in the NFC network in thin films obtained by filtration or casting.[5,17] In the nanocomposites containing 60 vol % unmodified NFC [Figure 5(b)], NFC-rich sheets appeared to alternate with matrix-rich layers and fracture took place after extensive sliding between these layers. In the MPS-modified NFC nanocomposites [Figure 5(d)], the layered structure was still apparent, but the fibrils were more uniformly distributed in the matrix. Finally, in the CAN-modified NFC nanocomposites [Figure 5(f)], the layered structure was further disrupted, as suggested by the relatively uniform roughness of the fracture surface. Although the morphology seen in Figure 5 may have been influenced by additional factors (microdeformation mechanisms, fracture mode, etc.), it is concluded that chemical treatment of the NFC, and treatment with CAN in particular, led to relatively homogeneous morphologies. In the case of CAN, grafting of HBP molecules to the cellulose surface during the drying step is thought to prevent collapse/aggregation of the nanofibrils as the solvent evaporates.

Thermomechanical Properties

The in-plane storage moduli, loss moduli and loss tangent, tan δ, measured by DMTA for the different materials are given in Figure 6. The HBP showed an α-transition temperature, T_α, at around 75°C (temperature of the tan δ peak associated with the glass transition in amorphous polymers). The storage modulus of about 1.5 GPa in the glassy state dropped to 40 to 50 MPa at

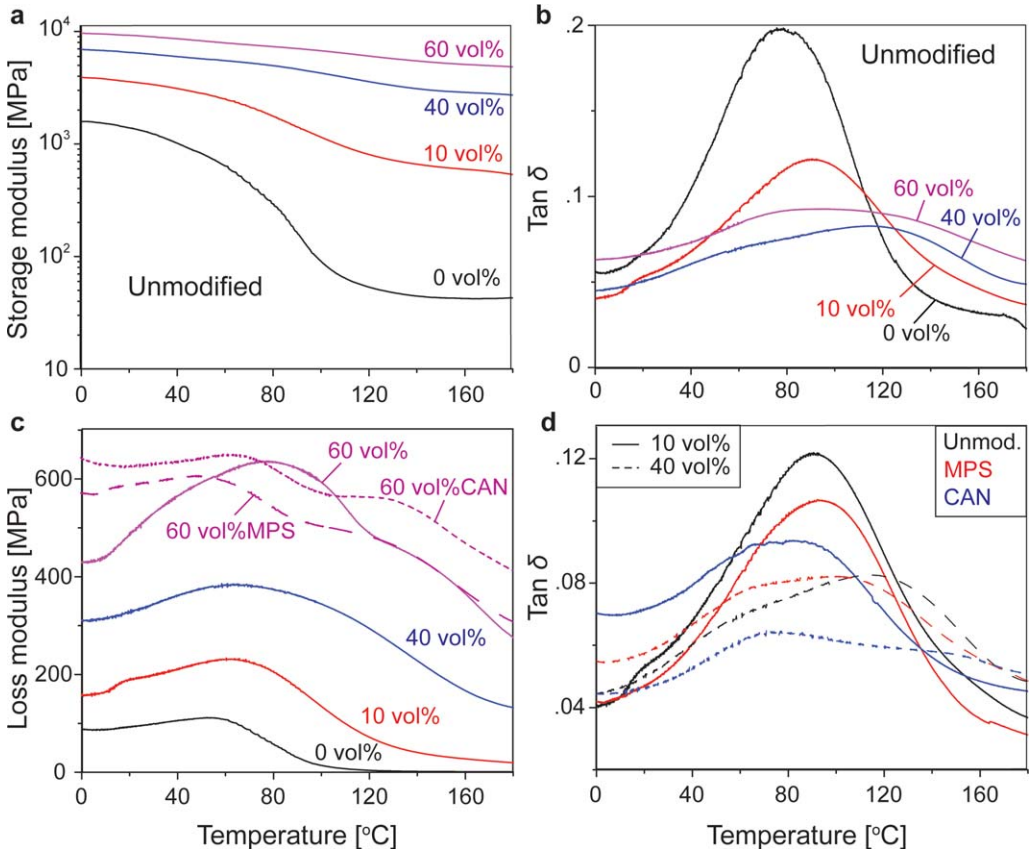

Figure 6. Storage (a) and loss (c) moduli, and tan δ (b, d) for nanocomposites with different NFC contents and chemical treatments. [Color figure can be viewed in the online issue, which is available at wileyonlinelibrary.com.]

temperatures above T_α [Figure 6(a)]. The addition of NFC significantly increased the storage modulus over the whole temperature range, the glassy modulus reaching approximately 10 GPa for the nanocomposite containing 60 vol % unmodified NFC (a six to sevenfold increase over that of the resin). The relative increase in storage modulus was even greater in the rubbery regime, its reaching roughly two orders of magnitude on addition of 60 vol % unmodified NFC to the HBP (6 to 7 GPa). Such observations are typical of NFC-reinforced polymer matrixes[15,39] and may be explained by the weak dependence of the stiffness of the cellulose nanofibril network (crystal modulus of about 100 GPa[40,41]) on temperature in the range considered.

The intensity of the peak in tan δ characteristic of the α-transition was also significantly reduced in the presence of NFC [Figure 6(b)]. Moreover, T_α shifted to higher temperatures (to 90°C at 10 vol % and to 120°C at 40 vol % NFC [Figure 6(b)]), as reflected by both tan δ and the loss modulus [Figure 6(c)], indicating a marked decrease in the molecular mobility of the polymer network. These results are consistent with the observation by photocalorimetry of a decrease in α_{vitr} on addition of NFC, but a constant maximum conversion [Figure 4(a)]. A greater amount of conversion therefore took place in the glassy state, which is expected to result in higher thermal stability of the final polymer network.[39]

The influence of NFC treatment on the thermomechanical behavior of the nanocomposites was most evident from the loss modulus and tan δ [Figure 6(c,d)]. While the tan δ peak for the MPS-modified NFC was not very different from that for the unmodified NFC at low NFC contents (10 vol %), its amplitude was significantly reduced for the CAN-modified NFC [Figure 6(d)]. At higher NFC contents (40 and 60 vol %), the nanocomposites apparently showed two overlapping tan δ and loss modulus peaks [Figure 6(d)], although this effect was most marked for the CAN- and MPS-modified NFC. In each case, the tan δ peak could be fitted with two Gaussian peaks, with a low temperature peak centered at 65 to 70°C for all the nanocomposites, and a high temperature peak at roughly 110, 120, and 130°C with 60 vol % MPS-modified, unmodified and CAN-modified NFC respectively. This suggests the coexistence of two matrix phases:[16,42] a bulk phase with a T_α close to that of the resin, and an interphase associated with the NFC surface with reduced mobility and hence a higher T_α.

In the case of CAN-modified NFC, free radical polymerization initiated from the cellulose surface (for the most part before photopolymerization of the bulk HBP), and the direct covalent attachment of HBP oligomers to the cellulose surface may be invoked to explain the relatively low mobility of the interphase. The more limited reduction in mobility of the interphase after modification with MPS might be attributed to reduced covalent bonding between the HBP and the MPS-modified NFC, possibly owing to competition with bulk polymerization of the HBP, which in this case took place at the same time as the coupling

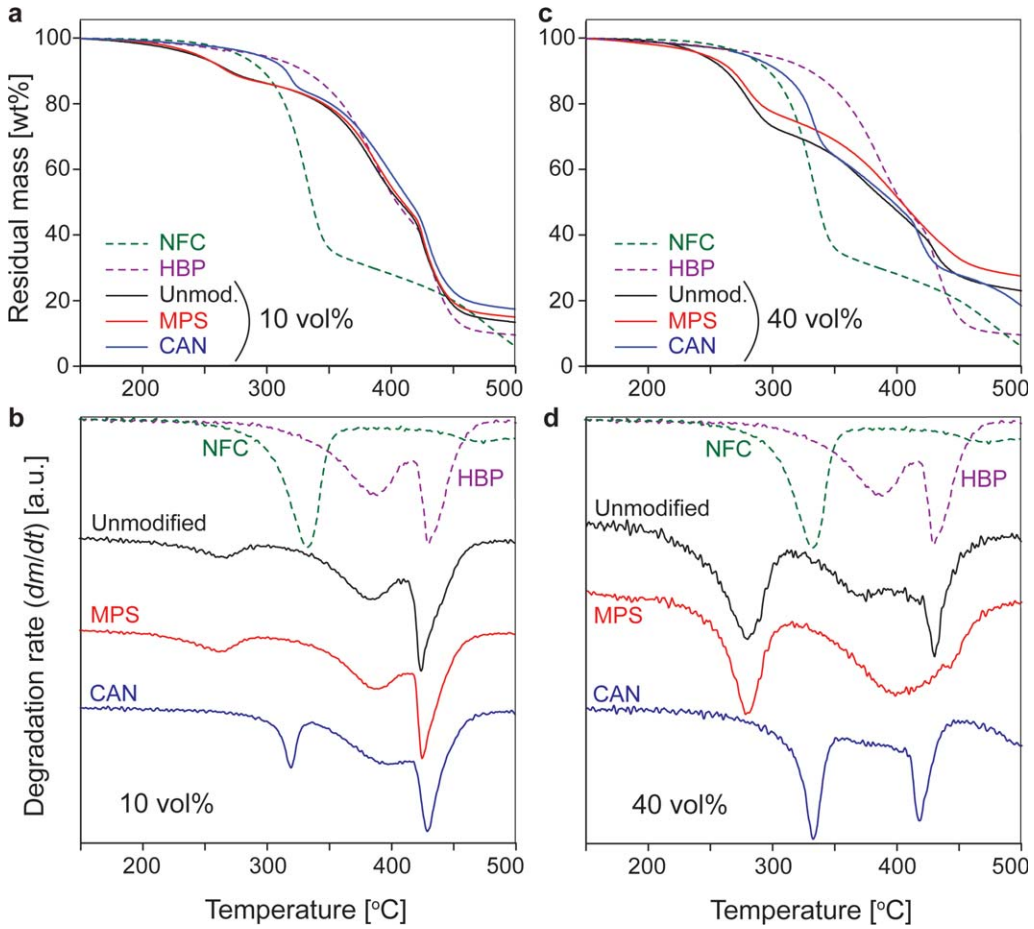

Figure 7. TGA curves of the weight loss (a, b) and its derivative (c, d) as a function of temperature for samples with 10 (a, c) and 40 (b, d) vol % NFC (various treatments); the dashed lines refer to data for the reference specimens (100% NFC and 100% HBP). [Color figure can be viewed in the online issue, which is available at wileyonlinelibrary.com.]

reaction. The aliphatic moieties associated with the MPS may also serve to decouple the covalently bonded HBP from the rigid cellulose substrate, reducing the influence of this latter on the mobility of the interphase. That the tan δ peaks for the nanocomposites containing unmodified NFC were generally similar to those obtained with the MPS-modified NFC (e.g. a significantly higher T_α than in the absence of NFC), suggests strong secondary interactions (e.g. hydrogen bonds) at the cellulose-HBP interface in the dry state, even in the absence of chemical modification (the DMTA measurements were made under ambient conditions, i.e. relatively dry at the temperatures in question).

Thermogravimetric Analysis

The thermal degradation of the various materials in an oxidative atmosphere is shown in Figure 7. The onset of degradation in 100% NFC occurred at about 250°C, with a maximum degradation rate at about 330°C. The HBP degraded in two stages, starting at about 300°C, with two peaks in the degradation rate at 380 and 430°C. In the nanocomposites, these three peaks in the degradation rate were generally identifiable, their intensity varying according to the NFC content. There was also a strong shift in the peak in the NFC degradation rate to lower temperatures (ca. 270°C) for the unmodified and MPS-modified NFC, but not for the CAN-modified NFC. Moreover, the low temperature peak in the degradation rate of the resin was suppressed in the presence of 40 wt % CAN-modified NFC [Figure 7(d)], so that matrix degradation took place in a single step at 420°C. At 40 wt % MPS-modified NFC, the two peaks characteristic of degradation of the neat HBP appeared to merge into a single, relatively broad peak centered at about 400°C, whereas the unmodified NFC had little effect, even at relatively high concentrations. While it is beyond the scope of the present work to attempt a detailed discussion of these trends, it is reasonable to assume that the globally higher oxygen permeability of the nanocomposites compared with that of the neat NFC (see the following section) contributed to the accelerated degradation of the cellulose in the presence of the HBP. Similar behavior has been observed in various open cellulose network materials, such as bacterial cellulose pellicles[43] and cellulose nanocrystal aerogels,[44] in which thermal degradation initiates at lower temperatures (ca. 250°C) than for a densely packed nanopaper (ca. 300°C). Even so, any such effect was clearly less marked in the case of the CAN-modified NFC, from which one may conclude that treatment of the NFC with CAN significantly improved its intrinsic thermal stability.

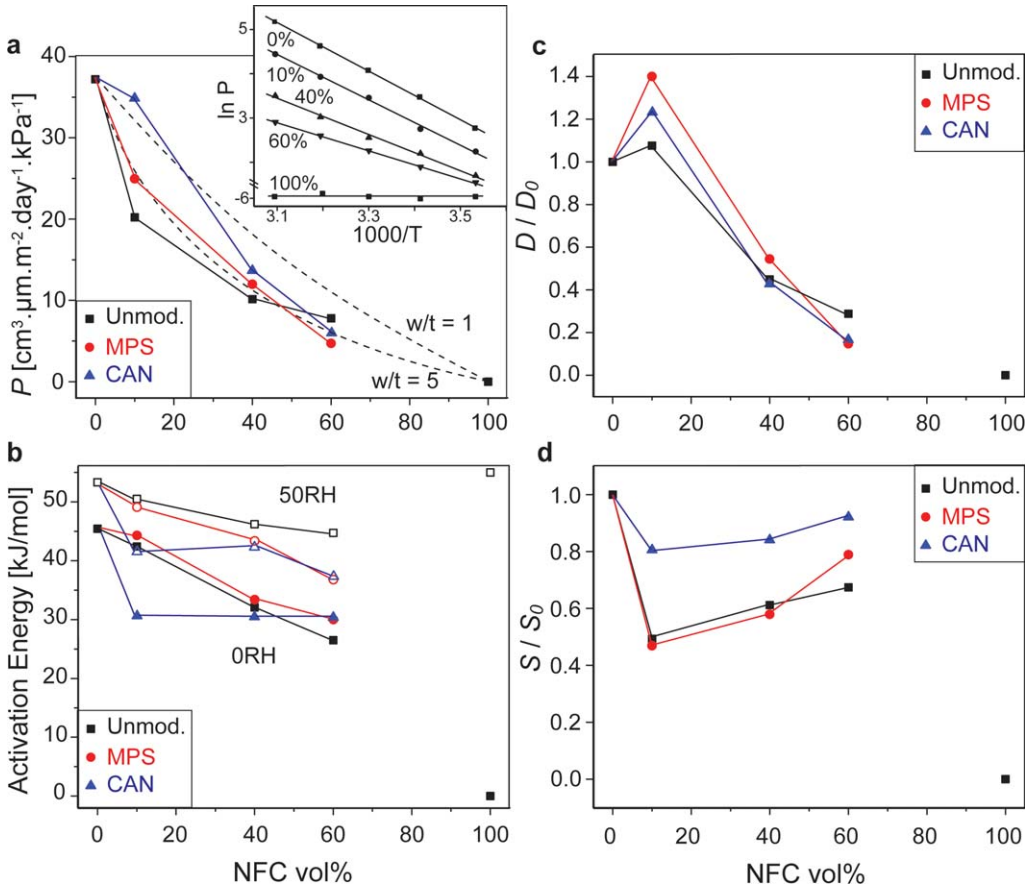

Figure 8. Permeability at 23°C and 0% RH (a), activation energies (b, filled symbols for 0% RH, open symbols for 50% RH), and relative diffusion (c) and solubility (d) coefficients (both at 0% RH), as a function of NFC vol % in all the nanocomposites. The dotted lines in (a) represent the permeability predicted from simple geometrical tortuosity models based on the assumption of different concentrations of impermeable ribbon-like inclusions with the different width/thickness ratios shown.[42] The inset in (a) shows the temperature dependence of the permeability for the unmodified nanocomposites in an Arrhenius plot. [Color figure can be viewed in the online issue, which is available at wileyonlinelibrary.com.]

Oxygen Barrier Properties Under Dry Conditions (0% RH)

Results from the oxygen permeability measurements are shown in Figure 8. The permeability of the HBP was 37 cm^3 µm m^{-2} day^{-1} kPa^{-1} at 23°C and in the dry state (0% RH), while a reference nanopaper (100% NFC) had a permeability of only 0.002 cm^3 µm m^{-2} day^{-1} kPa^{-1} under the same conditions. Excellent gas barrier properties have been reported previously for a dense network of highly crystalline dry cellulose nanofibrils.[8,11] All the HBP-NFC nanocomposites showed lower permeability than the HBP, and the permeability decreased as the NFC content was raised [Figure 8(a)]. Of the different chemical NFC treatments, the unmodified NFC provided the best barrier properties at 10 vol % loading (an approximately two-fold reduction in permeability with respect to the HBP). At this loading, the permeability with the CAN-modified NFC was only slightly lower than that of the HBP, while treatment with MPS led to intermediate behavior. At 40 vol % NFC content, the differences were less marked although the ranking of the barrier performance of the various materials remained the same. At 60 vol % loading, on the other hand, the modified NFC led to better barrier performance than the unmodified NFC.

Several models have been developed to predict the influence of discrete impermeable inclusions on the permeability of polymer nanocomposites.[45–49] However, their development has so far mainly focused on nanocomposites with platelet-shaped nanoparticles (e.g. clays) and an analytical model for the permeability of nanofiber network-based composites is to our knowledge lacking in the literature. Nielsen[45] derived the permeability for a material composed of a continuous matrix with impermeable ribbon-like particles distributed in a random array [eq. (5)],

$$\frac{P_0}{P} = \frac{\left(1+\frac{1}{3}\cdot\frac{w}{t}\cdot V_f\right)^2}{1-V_f} \tag{5}$$

where P_0 and P are the permeability of the matrix and the composite, respectively, w/t is the ribbon aspect ratio (width over thickness) and V_f is the particle volume fraction. This model is based on purely geometrical considerations, taking into account the increased path length (tortuosity) for a gas molecule crossing the nanocomposite membrane. Because the cellulose nanofibrils have a roughly square cross-section, they may be approximated to by ribbons with aspect ratio of 1. As seen in Figure 8(a), the experimental permeabilities were well below the predicted values (except for 10 vol % CAN-modified NFC), a

more satisfactory fit to most of the data requiring a ribbon aspect ratio of 5. NFC networks obtained by filtration techniques are known to exhibit preferential aggregation of the fibrils into two-dimensional sheets[5,15] (as confirmed by the present SEM observations in Figure 5), which may provide a physical interpretation to the apparently higher effective aspect ratio. However, as will be discussed in what follows, it is not clear that any such approach is able to account for all aspects of the observed behavior.

In the simplified representation used to derive apparent diffusion and solubility coefficients using the time-lag method (see the Experimental section), the diffusion coefficient represents dynamic mass transport phenomena, whereas the solubility coefficient gives the concentration of oxygen absorbed by the polymer at a given oxygen partial pressure at thermodynamic equilibrium.[32] Figure 8(c,d) show the calculated apparent coefficients for the different composite materials (at 23°C), normalized with respect to those obtained for the pure HBP. Surprisingly, the diffusion coefficient [Figure 8(c)] increased slightly on addition of 10 vol % NFC, although it decreased monotonically with further increases in NFC content. Hence, while impermeable second phase inclusions may act as diffusion barriers even at low concentrations, this was clearly not the dominant effect at 10 vol % NFC, particularly when the NFC was modified with MPS or CAN. Departures from tortuosity models in nanocomposites are often attributed to changes in the viscoelastic response of the matrix, which is intimately linked to rates of mass transport. While the overall decreases in matrix mobility with NFC content implied by the results in Figure 6 would generally be expected to reinforce the tortuosity effect, it is perhaps significant that the values of tan δ at temperatures below T_α in some cases exceeded those for the neat HBP (cf. the results for 10 vol % CAN-modified NFC), suggesting a more complex dependence of the effective matrix mobility on NFC content than implied by the simple two-phase model referred to previously. Another possibility is that defects at the nanofibril-matrix interface act to bridge regions of locally high matrix mobility,[50] resulting in a percolating permeable pathway at low NFC contents, the effects of which nevertheless become dominated by tortuosity and matrix immobilization as the NFC content increases. However, regardless of such speculations, which cannot be substantiated further on the basis of the present results, particularly in view of other potential contributing factors such as variations in the homogeneity of the NFC dispersion, the overall trend is for the oxygen diffusion rate to decrease strongly at high NFC contents, tending towards that of the pure NFC nanopaper.

It follows from the dependence of the diffusion coefficient on NFC content that the apparent solubility coefficient of the composite [Figure 8(d)] decreased sharply on addition of 10 vol % NFC, the effect being most marked for the neat and MPS-modified NFC. The solubility coefficient then increased somewhat on further addition of NFC. Such behavior is again inconsistent with a geometrical model, which would imply a linear relationship between the solubility coefficient and the volume fraction of impermeable inclusions. A significant decrease in the intrinsic oxygen solubility of the HBP might be accounted for in terms of the decreased chain mobility inferred from the results of the thermomechanical analysis. However, the observed increase in oxygen solubility at higher NFC, is more difficult to account for in terms of the intrinsic materials response. One possibility is that extrinsic defects, such as microvoids formed at the fibril/matrix interface and within fibril/fibril aggregates during drying may contribute to oxygen uptake at high NFC contents, because oxygen is expected to adsorb strongly to accessible NFC surfaces.[51] Similar effects have been observed in certain clay-based polymer nanocomposites, in which the moisture uptake as a function of clay content passes through a minimum at low clay contents,[52] and have been argued to reflect defects associated with aggregate formation. Such defects do not necessarily contribute to diffusion, given that they are associated with relatively impermeable regions of the nanocomposites. In the case of the CAN-modified NFC, the solubility was higher, in spite of the improved NFC dispersion. This may be due to the different polymerization route (i.e. grafting from NFC surface during solvent evaporation, followed by UV irradiation), leading to a less compact cellulose nanofiber network [see Figure 5(f) vs. 5(b)] and a relatively high proportion of microvoids.

Activation energies for oxygen permeation were also measured in the temperature range 10 to 50°C for the various materials, both under dry conditions (0% RH) and at 50% RH. The temperature dependence of permeability could be accurately represented by an Arrhenius law [Figure 8(a)],

$$P = A \cdot e^{-\frac{E_a}{RT}} \tag{6}$$

where A is the pre-exponential factor, E_a is the activation energy, R is the universal gas constant, and T is the absolute temperature. In the dry state, the activation energy of the specimens containing unmodified and MPS-modified NFC decreased almost linearly with NFC content from about 45 kJ mol^{-1} to an effective value of 0 kJ mol^{-1} for the pure nanopaper. The CAN-modified NFC, on the other hand, gave an activation energy of about 30 kJ mol^{-1} at all volume fractions [Figure 8(b)]. Thermal activation results in increased polymer chain mobility at elevated temperatures, leading to higher diffusion rates. However, given that the permeability of the highly crystalline nanofibrils was not significantly affected in the temperature range considered (<50°C), the consequent reduction in activation energy in the presence of NFC therefore indicates a positive influence of this latter on the thermal stability of the oxygen barrier properties, which may be linked in turn to the improvements in thermomechanical properties discussed previously.

Oxygen Barrier Properties and Moisture Adsorption Under Wet Conditions

The effect of relative humidity on oxygen permeability is shown in Figures 9 and 10, together with the moisture uptake at the corresponding relative humidity. The HBP exhibited significant moisture adsorption (up to 2.8 wt % at 80% RH), accounting for the observed increase in permeability from 37 cm^3 μm m^{-2} day^{-1} kPa^{-1} at 0% RH to 46 cm^3 μm m^{-2} day^{-1} kPa^{-1} at 80 % RH

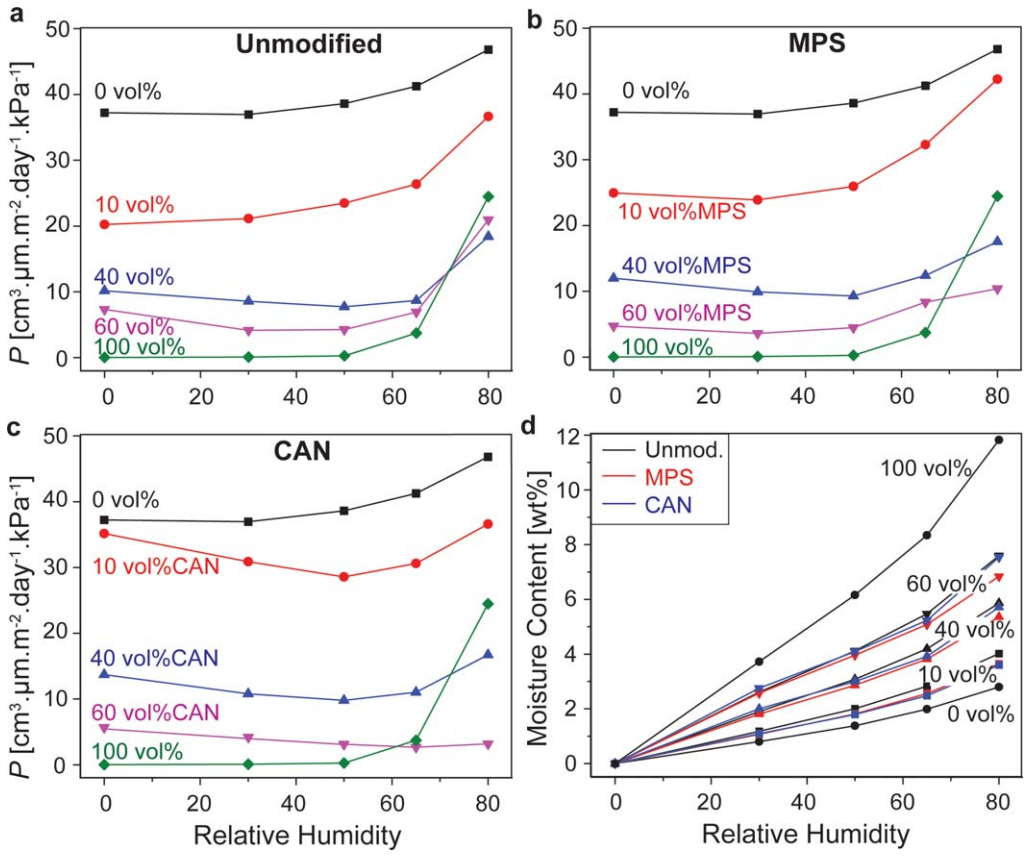

Figure 9. Effect of relative humidity (RH) on permeability (a, b, c) and moisture uptake (d) for the nanocomposites with unmodified (a), MPS-modified (b) and CAN-modified (c) NFC. [Color figure can be viewed in the online issue, which is available at wileyonlinelibrary.com.]

(a 25% increase). In contrast, the pure NFC nanopaper, as expected and as previously reported,[8] showed much stronger moisture sensitivity. At 50% RH and a 6.2 wt % moisture content, the permeability increased to 0.26 cm^3 µm m^{-2} day^{-1} kPa^{-1} (a 100-fold increase from its value at 0% RH), and on increasing the humidity to 80% RH (11.8 wt % moisture content) the permeability increased by two further orders of magnitude to about 24 cm^3 µm m^{-2} day^{-1} kPa^{-1}. For the HBP-NFC nanocomposites, the moisture content [Figure 9(d)] increased almost linearly from 0% to 80% RH, with levels intermediate between the ones for pure HBP and NFC. The influence of the chemical treatment was not clear-cut, but the modified NFC generally led to slightly lower moisture uptake than the non-modified NFC. As shown in Figure 9(a–c), the permeability changed relatively little in the 0 to 50% RH range but increased more strongly in the range 50 to 80% RH. However, in the samples with high NFC contents, there was a slight initial decrease in permeability with RH (with respect to the dry state). This phenomenon was both reproducible (there was no hysteresis on repeated drying) and unexpected. It is speculated to be due to microvoid formation owing to internal stresses at the cellulose/polymer interfaces in the fully dry state. Small amounts of moisture may occupy these microvoids and/or induce collapse of the pores by promoting stress relaxation of the polymer via plasticization, resulting in reduced oxygen permeability.

In spite of the limited differences in permeability between 0% and 50% RH, the activation energies were significantly higher at 50% RH [Figure 8(b)]. The activation energy of the composites at 50% RH decreased with NFC content, but was lower than for the pure NFC (55 kJ mol^{-1}) under the same conditions, suggesting a synergistic effect in the nanocomposites.

At high relative humidity (i.e. 80% RH), traditional cellulose-based materials are known to lose most of their exceptional properties (not only gas barrier properties, but also mechanical stiffness, for example). The adsorption of water molecules through hydrogen bonds to accessible cellulose surfaces (in amorphous regions and at fibril interfaces) is responsible for this plasticizing effect leading to reduced barrier and mechanical properties.[8] To compare the high humidity performance of the different materials investigated here, two indicators were selected: the permeability at 80% RH [P_{80RH}, Figure 10(a)] and the ratio between the maximum and minimum permeability [P_{max}/P_{min}, Figure 10(b)], which are representative of the absolute performance under moist conditions and the relative moisture stability, respectively.

At 10 and 40 vol % NFC, chemical treatment had little influence on P_{80RH} (P_{80RH} was about 19 cm^3 µm m^{-2} day^{-1} kPa^{-1} for all the nanocomposites at 40 vol % NFC, as compared to 46 and 24 cm^3 µm m^{-2} day^{-1} kPa^{-1} for the HBP and pure NFC). The nanocomposites were therefore better barriers under moist

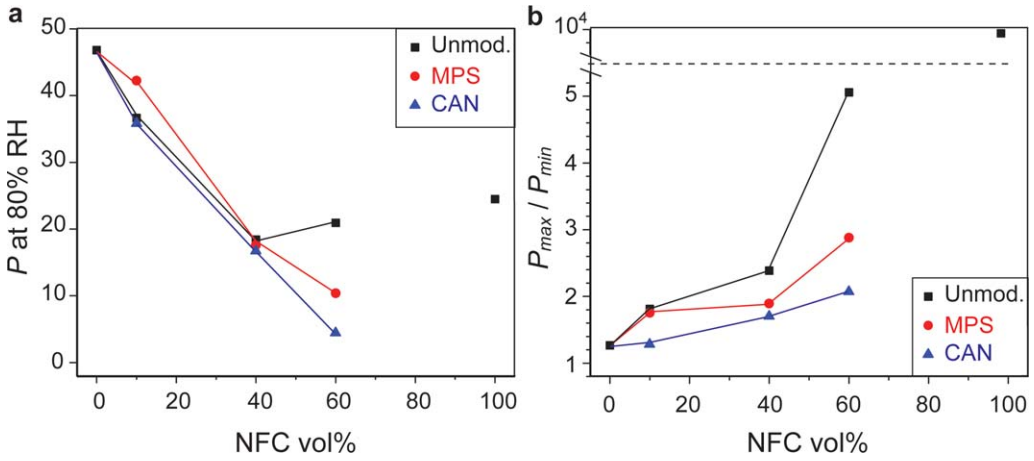

Figure 10. Evolution of the permeability at high RH (a) and of the relative variation in permeability (P_{max}/P_{min}) (b) as a function of NFC content (various treatments). [Color figure can be viewed in the online issue, which is available at wileyonlinelibrary.com.]

conditions than the neat components, i.e. there was again evidence of synergy between the matrix and the NFC. Hence the homogeneous nanocomposites prepared here should perform better at high humidity than hypothetical multilayer films with the same compositions (e.g. a nanopaper coated with HBP).

At 60 vol % NFC, the influence of the chemical treatment on P_{80RH} was more marked. While the permeability was somewhat greater for 60 vol % nonmodified NFC than for 40 vol % nonmodified NFC, it decreased for the modified NFC, particularly in the case of CAN, for which P_{80RH} was about 5 cm^3 µm m^{-2} day^{-1} kPa^{-1}. This may be due to better compatibility between the polymer matrix and the cellulose fibrils, reduced fibril aggregation, and/or extensive hydrophobization of the cellulose surfaces. Microvoids and porosity, which are likely to be present at high NFC contents (e.g. within fibril aggregates/bundles), are expected to provide preferred sites for moisture adsorption at the cellulose surface, leading to poorer barrier properties and implying a link with the proposed mechanism for increased oxygen solubility described previously (i.e. adsorption to accessible NFC surface within aggregates). The benefit of the chemical treatments is even more obvious if one considers the relative moisture stability [P_{max}/P_{min}, Figure 10(b)]. P_{max}/P_{min} increased steadily with addition of unmodified NFC up to about 5 at 60% loading. For the MPS-modified NFC, it remained below 3 and it reached a maximum of only 2 for the CAN-modified NFC. Thus, one of the most interesting effects of the chemical surface modification investigated in this work was significantly reduced moisture sensitivity of the gas barrier properties, particularly at high NFC loadings.

CONCLUSIONS

A photopolymerizable hyperbranched acrylate resin was used to impregnate wet cellulose nanofibril network templates and prepare homogeneous nanocomposite films by rapid UV cure. The NFC template could be chemically modified before impregnation with the resin, in order to introduce either a methacrylated silane coupling agent (MPS route) or directly grafted HBP oligomers (CAN route) to the fiber surfaces. The success of these two types of modification was confirmed and the presence of NFC and MPS-modified NFC was found not to affect the photopolymerization kinetics, regardless of the composition. On the other hand, CAN served as a highly efficient free-radical initiator even under ambient conditions, so that substantial polymerization of the HBP took place before UV exposure.

The homogeneous dispersion of the impermeable cellulose nanofibrils in the HBP matrix resulted in significantly improved oxygen barrier properties, e.g. an 80% reduction in dry permeability with 60 vol % modified NFC. However, the most important results were obtained from permeation tests at high relative humidity. Neat NFC networks are known to lose their excellent gas barrier properties in wet conditions as was confirmed here. On the other hand, all the nanocomposites showed significantly reduced moisture sensitivity, thanks to the use of a relatively hydrophobic matrix to embed the NFC. Moreover, the chemical treatments provided further enhancements in the moisture stability, particularly at high NFC contents, with the CAN-modified NFC showing the best performance in this respect. Thus, at 60 vol % of CAN-modified NFC, the permeability at 80% RH was only 5 cm^3 µm m^{-2} day^{-1} kPa^{-1}, i.e. five times lower than that of the neat NFC nanopaper membrane under the same conditions and almost 10 times lower than that of the neat HBP. Indeed, over the whole range of relative humidity considered (0 to 80%), the permeability only varied by a factor 2 for this composition (as compared with a factor of 10,000 for the neat NFC nanopaper).

Separation of the dynamic diffusion and steady state solubility contributions to the permeation process using the time-lag method revealed some unexpected trends, namely a highly nonlinear response of the solubility coefficient to NFC addition, and an increase in diffusion coefficient at low NFC contents. These results indicated a complex interplay between the HBP matrix and the NFC nanofibrils that cannot be accounted for by conventional models for permeation in nanocomposites based on purely geometrical considerations.

The thermal stability and thermomechanical properties were also strongly improved by addition of NFC to the HBP,

suggesting a sharp reduction in polymer chain mobility, as evidenced by increases in T_α and much higher storage moduli above the glass transition temperature. Moreover, the α-transition at 40 vol % NFC or more was characterized by two distinct tan δ peaks that could be assigned to a bulk polymer phase (T_α of around 70°C) and an immobilized interphase (T_α from 110 to 130°C depending on chemical treatment of the NFC).

In summary, this work has demonstrated cellulose nanofibrils to have considerable potential for the combined improvement of oxygen barrier and thermomechanical properties of a polymer matrix. The wet template impregnation route developed for the photopolymerizable resin provides a homogeneous NFC dispersion in the matrix, and it should be possible to adapt this approach to a large scale roll-to-roll process by shortening the processing times further (rapid UV cure). Moreover, we have shown that the moisture sensitivity generally associated with cellulose-based nanocomposites may be drastically reduced by appropriate chemical modification of the wet template.

ACKNOWLEDGMENTS

The Knut and Alice Wallenberg Foundation is acknowledged for its financial support to the Wallenberg Wood Science Center (WWSC). The SEM observations were carried out at the EPFL Interdisciplinary Center for Electron Microscopy (CIME).

REFERENCES

1. DeLassus, P. In Kirk-Othmer Encyclopedia of Chemical Technology; John Wiley and Sons, New-York, **2000**.
2. Priolo, M. A.; Holder, K. M.; Greenlee, S. M.; Grunlan, J. C. *ACS Appl. Mater. Interfaces* **2012**, *4*, 5529.
3. Yang, Y. -H.; Bolling, L.; Priolo, M. A.; Grunlan, J. C. *Adv. Mater.* **2013**, *25*, 493.
4. Leterrier, Y. *Prog Mater. Sci.* **2003**, *48*, 1.
5. Henriksson, M.; Berglund, L. A.; Isaksson, P.; Lindström, T.; Nishino, T. *Biomacromolecules* **2008**, *9*, 1579.
6. Eichhorn, S. J.; Dufresne A.; Aranguren M.; Marcovich N. E.; Capadona J. R.; Rowan S. J.; Weder C.; Thielemans W.; Roman M.; Renneckar S.; Gindl W.; Veigel S.; Keckes J.; Yano H.; Abe K.; Nogi M.; Nakagaito A. N.; Mangalam A.; Simonsen J.; Benight A. S.; Bismarck A.; Berglund L. A.; Peijs T. *J. Mater. Sci.* **2009**, *45*, 1.
7. Nogi, M.; Iwamoto, S.; Nakagaito, A. N.; Yano, H. *Adv. Mater.* **2009**, *21*, 1595.
8. Aulin, C.; Gällstedt, M.; Lindström, T. *Cellulose* **2010**, *17*, 559.
9. Aulin, C.; Karabulut, E.; Tran, A.; Wågberg, L.; Lindström, T. *ACS Appl. Mater. Interfaces* **2013**, *5*, 7352.
10. Siró, I.; Plackett, D.; Hedenqvist, M.; Ankerfors, M.; Lindström, T. *J. Appl. Polym. Sci.* **2011**, *119*, 2652.
11. Belbekhouche, S.; Bras, J.; Siqueira, G.; Chappey, C.; Lebrun, L.; Khelifi, B.; Marais, S.; Dufresne, A. *Carbohydr. Polym.* **2011**, *83*, 1740.
12. Fukuzumi, H.; Saito, T.; Iwata, T.; Kumamoto, Y.; Isogai, A. *Biomacromolecules* **2009**, *10*, 162.
13. Lavoine, N.; Desloges, I.; Dufresne, A.; Bras, J. *Carbohydr. Polym.* **2012**, *90*, 735.
14. Plackett, D.; Anturi, H.; Hedenqvist, M.; Ankerfors, M.; Gällstedt, M.; Lindström, T.; Siró, I. *J. Appl. Polym. Sci.* **2010**, *117*, 3601.
15. Sehaqui, H.; Zhou, Q.; Berglund, L. A. *Soft Matter* **2011**, *7*, 7342.
16. Henriksson, M.; Fogelström, L.; Berglund, L. A.; Johansson, M.; Hult, A. *Compos. Sci. Technol.* **2011**, *71*, 13.
17. Ansari, F.; Galland, S.; Johansson, M.; Plummer, C. J. G.; Berglund, L. A. To appear.
18. Sharma, H.S.S.; Carmichael, E.; Muhamad, M.; McCall D.; Andrews, F.; Lyons, G.; McRoberts, W. C.; Hornsby, P. R. *RSC Adv.* **2012**, *2*, 6424.
19. Pan, H.; Song, L.; Ma, L.; Hu, Y. *Ind. Eng. Chem. Res.* **2012**, *51*, 16326.
20. Henriksson, M.; Henriksson, G.; Berglund, L. A.; Lindström, T. *Eur. Polym. J.*, **2007**, *43*, 3434.
21. Sun, C. C. *J. Pharm. Sci.* **2005**, *94*, 2132.
22. Xie, Y.; Hill, C. A. S.; Xiao, Z.; Militz, H.; Mai, C. *Compos. A* **2010**, *41*, 806.
23. Abdelmouleh, M.; Boufi, S.; Belgacem, M. N.; Dufresne, A.; Gandini, A. *J. Appl. Polym. Sci.* **2005**, *98*, 974.
24. Lu, J.; Askeland, P.; Drzal, L. T. *Polymer* **2008**, *49*, 1285.
25. Salon, M. -C. B.; Gerbaud, G.; Abdelmouleh, M.; Bruzzese, C.; Boufi, S.; Belgacem, M. N. *Magn. Reson. Chem.* **2007**, *45*, 473.
26. Littunen, K.; Hippi, U.; Johansson, L. -S.; Österberg, M.; Tammelin, T.; Laine, J.; Seppälä, J.; et al. *Carbohydr. Polym.* **2011**, *84*, 1039.
27. Shukla, S. R.; Athalye, A. R. *J. Appl. Polym. Sci.* **1994**, *54*, 279.
28. Kubota, H.; Ogiwara, Y. *J. Appl. Polym. Sci.* **1970**, *14*, 2611.
29. Geiser, V.; Leterrier, Y.; Månson, J. -A. E. *J. Appl. Polym. Sci.* **2009**, *114*, 1954.
30. Geiser, V.; Leterrier, Y.; Månson, J. -A. E. *Macromol. Mater. Eng.* **2012**, *297*, 155.
31. Anseth, K. S.; Wang, C. M.; Bowman, C. N. *Polymer* **1994**, *35*, 3243.
32. Felder, R. M. *J. Membr. Sci.* **1978**, *3*, 15.
33. Geiser, V. R.; Leterrier, Y.; Månson, J. -A. E. *Macromolecules* **2010**, *43*, 7705.
34. Pääkkö, M. et al. *Biomacromolecules* **2007**, *8*, 1934.
35. Keenan, M. R. *J. Appl. Polym. Sci.* **1987**, *33*, 1725.
36. Schmidt, L.; Schmäh, D.; Leterrier, Y.; Månson, J. -A. *Rheol. Acta* **2007**, *46*, 693.
37. Hon, N.-S. *J. Polym. Sci. Part A: Polym. Chem.* **1976**, *14*, 2497.
38. Davidson, R.S. *J. Photochem Photobiol B* **1996**, *33*, 3.
39. Azizi Samir, M. A. S.; Alloin, F.; Paillet, M.; Dufresne, A. *Macromolecules* **2004**, *37*, 4313.

40. Sakurada, I.; Nukushina, Y.; Ito, T. *J. Polym. Sci.* **1962**, *57*, 651.
41. Wohlert, J.; Bergenstråhle-Wohlert, M.; Berglund, L. *Cellulose* **2012**, *19*, 1821.
42. Tsagaropoulos, G.; Eisenberg, A. *Macromolecules* **1995**, *28*, 6067.
43. Zhijiang, C.; Guang, Y. *J. Appl. Polym. Sci.* **2011**, *120*, 2938.
44. Smith, S. W.; Chan, H.; Buesch, C.; Simonsen, J.; Conley, J. F. *MRS Proc.* **2012**, *1465*.
45. Lape, N. K.; Nuxoll, E. E.; Cussler, E. L. *J. Membr. Sci.* **2004**, *236*, 29.
46. Takahashi, S.; Goldberg, H. A.; Feeney, C. A.; Karim, D. P.; Farrell, M.; O'Leary, K.; Paul, D. R. *Polymer* **2006**, *47*, 3083.
47. Nielsen, L. E. *J. Macromol. Sci. A* **1967**, *1*, 929.
48. Gusev, A. A.; Lusti, H. R. *Adv. Mater.* **2001**, *13*, 1641.
49. Fredrickson, G. H.; Bicerano, J. *J. Chem. Phys.* **1999**, *110*, 2181.
50. Zhong, J.; Wen Jones, A. A. *Macromolecules* **2003**, *36*, 6430.
51. Orr, R. G. Gas Adsorption on Wood Cellulose; PhD Thesis; University of British Columbia: British Columbia, **1970**.
52. Muralidharan, M. N.; Kumar, S. A.; Thomas, S. *J. Membr. Sci.* **2008**, *315*, 147.